

# Solid acids with SO<sub>3</sub>H groups and tunable surface properties: versatile catalysts for biomass conversion†

Cite this: *J. Mater. Chem. A*, 2014, 2, 11813

P. A. Russo,<sup>‡a</sup> M. M. Antunes,<sup>‡a</sup> P. Neves,<sup>a</sup> P. V. Wiper,<sup>a</sup> E. Fazio,<sup>b</sup> F. Neri,<sup>b</sup> F. Barreca,<sup>b</sup> L. Mafra,<sup>a</sup> M. Pillinger,<sup>a</sup> N. Pinna<sup>\*c</sup> and A. A. Valente<sup>\*a</sup>

Acid catalysis plays an important role in biomass conversion processes for producing chemicals and fuels. We report a relatively simple procedure for synthesizing versatile, strong acid catalysts based on carbon and carbon–silica composites with sulfonic acid groups. The process involves chemical activation of a sulfonic acid organic precursor at low temperature. The synthesis conditions can be modified to tune the surface composition, texture, and the acid properties of the materials towards superior catalytic performances. Molecular level insights into the nature and strength of the acid sites were gained by combining high resolution XPS and <sup>1</sup>H-decoupled <sup>31</sup>P MAS NMR spectroscopy of adsorbed triethylphosphine oxide. These materials are effective acid catalysts for the conversion of different biomass-derived chemicals to useful bio products such as furanic ethers and levulinate esters.

Received 8th May 2014  
Accepted 2nd June 2014

DOI: 10.1039/c4ta02320j

www.rsc.org/MaterialsA

## Introduction

Intensive research efforts are being devoted to the development of sustainable routes for producing chemicals and fuels. The use of renewable feedstocks and heterogeneous catalytic processes are making a significant contribution to accomplishing this goal.<sup>1–3</sup> In this context, there is strong interest in developing efficient and stable heterogeneous acid catalysts, since they are more environmentally friendly than their homogeneous analogues and a wide range of important industrial reactions are catalyzed by acids.<sup>2,4</sup>

Carbon-based materials containing sulfonic acid (SO<sub>3</sub>H) groups are especially attractive catalysts due to their low cost, metal-free composition, and expected high stability and strong acidity. Therefore, the synthesis and catalytic properties of several types of carbon-based materials modified with SO<sub>3</sub>H groups have recently been reported.<sup>5–18</sup> In particular, the sulfonation of carbons synthesized by incomplete carbonization (below *ca.* 450 °C)<sup>4,5,11–13</sup> or hydrothermal carbonization (below *ca.* 250 °C)<sup>14,17,19–21</sup> of organic matter can generate solids with high contents of acid functionalities (<2.5 mmol g<sup>−1</sup> of COOH,

SO<sub>3</sub>H and OH). Indeed, materials produced by the former approach have shown very promising catalytic activity for many acid-catalyzed reactions, performing better, for example, in the hydrolysis of cellulose and production of biodiesel, than commercial catalysts like zeolites, niobic acid or Amberlyst-15.<sup>5,12,22</sup> However, carbons prepared by partial carbonization of organic molecules have extremely low surface areas (<10 m<sup>2</sup> g<sup>−1</sup>). If the reactants are unable to reach the acid sites in the bulk, the low surface area available for reaction leads to poor catalytic activity. This problem can be overcome by depositing the carbon precursor over a large surface area silica prior to carbonization.<sup>15</sup> Additionally, the catalyst morphology and porosity can be controlled, with the silica providing mechanical stability.<sup>16,23</sup> An important requirement for sulfonated carbon catalysts is stability towards leaching of sulfur-containing species into the reaction mixtures, which is not easily accomplished and has detrimental effects on the catalytic performances.<sup>10,20,24,25</sup> This problem can be pronounced for solids prepared at low temperatures. Moreover, the functionalization with SO<sub>3</sub>H groups is frequently accomplished by heating the carbon in large volumes of concentrated H<sub>2</sub>SO<sub>4</sub> or fuming H<sub>2</sub>SO<sub>4</sub> (*ca.* ≥20 mL to 1 g of solid) above 150 °C, which is a hazardous process that generates large amounts of neutralization wastes. Therefore, synthesis procedures have recently been developed in order to eliminate this step.<sup>14,16,21,26</sup> Carbons with SO<sub>3</sub>H groups were prepared by hydrothermal carbonization of mixtures of organic compounds including glucose, resorcinol, furaldehyde, *p*-toluenesulfonic acid and hydroxyethylsulfonic acid.<sup>14,20,21,26</sup> The resulting solids exhibited interesting catalytic performances, but leaching of sulfur-containing moieties was problematic for some of the materials.<sup>20</sup>

<sup>a</sup>Department of Chemistry, CICECO, University of Aveiro, Campus de Santiago, 3810-193 Aveiro, Portugal. E-mail: atav@ua.pt

<sup>b</sup>Università degli Studi di Messina, Dipartimento di Fisica e di Scienze della Terra, Viale F. Stagno d'Alcontres, 31 98166 Messina, Italy

<sup>c</sup>Institut für Chemie, Humboldt Universität zu Berlin, Brook-Taylor-Straße 2, 12489 Berlin, Germany. E-mail: nicola.pinna@hu-berlin.de

† Electronic supplementary information (ESI) available. See DOI: 10.1039/c4ta02320j

‡ P. A. R and M. M. A. contributed similarly to this work.



Chemical activation allows the production of carbons with controlled porosity.<sup>27–30</sup> This method involves the impregnation of a carbon or carbon precursor with a chemical agent followed by pyrolysis. Several chemicals can act as activating agents, with phosphoric acid and alkali metal hydroxides being the most widely used.<sup>27–30</sup> The pyrolysis is typically accomplished at lower temperatures and shorter times compared to common carbonization/physical activation processes, as the activating agent can promote the reactions involved in the transformation of the precursor into carbon (*e.g.* dehydrogenation or dehydration), as well as the formation of cross-links.<sup>28</sup> Herein, versatile carbon and carbon–silica composites containing sulfonic acid groups were prepared using a relatively simple procedure. The process involves chemical activation with H<sub>2</sub>SO<sub>4</sub> of a sulfonic acid organic precursor (*p*-toluenesulfonic acid) at low temperature. The prepared solid acids were tested as catalysts in the reactions of biomass-derived 5-hydroxymethyl-2-furaldehyde (HMF) and furfuryl alcohol (FA) with ethanol to give furanic ethers and levulinate esters (bioEs), as well as in the integrated conversion of fructose to bioEs (Fig. 1). Within a biorefinery, HMF and FA are derived from carbohydrates, the main components of lignocellulosic matter obtainable from forest,

agricultural, municipal and industrial wastes.<sup>1,3,31–37</sup> The bioEs have applications in different sectors of the chemical industry: levulinate esters can be used as solvents, plasticizing agents, odorous substances and fuel additives;<sup>38</sup> 5-(alkoxymethyl)-furfural products and the respective diacetals are interesting reagents for synthesizing surfactants;<sup>39</sup> particularly, ethyl levulinate (EL)<sup>40–43</sup> and 5-(ethoxymethyl)-furfural (5EMF)<sup>44</sup> possess interesting properties as oxygenated fuel extenders for gasoline, diesel and biodiesel. Amongst the most active solid acid catalysts for producing bioEs from saccharides,<sup>45–52</sup> HMF<sup>46,51–55</sup> and FA<sup>56–60</sup> are commercial ion-exchange resins such as Amberlyst™-15. Therefore, the catalytic performances of our catalysts were compared with this commercial acid resin.

## Experimental

### Preparation of the materials

In the synthesis of the carbon-silica composites (CST), 2.6 g of *p*-toluenesulfonic acid (TsOH; Panreac) was dissolved in acetone (Aldrich, 99.9%) and added to 1 g of fumed silica (Aldrich). The suspension was sonicated for 15 min, stirred for 24 h at room temperature and then heated at 100 °C for 6 h followed by 6 h at 160 °C. Subsequently, 10 mL of aqueous H<sub>2</sub>SO<sub>4</sub> with different concentrations (0.25, 1.0 and 2.5 M) was added to the pre-carbonized TsOH–silica solid. The amount of H<sub>2</sub>SO<sub>4</sub> was changed in order to obtain different ratios  $R$  = mass of chemical activating agent/mass of carbon precursor. The  $R$  values were varied between 0 and 1, where 0 corresponds to a non-activated material (just partially carbonized). The suspension was stirred at room temperature for 24 h and then the water was completely evaporated by heating at 110 °C. The acid impregnated solid was then thermally treated under nitrogen flow at 250 °C for 1 h in a tubular furnace. The final solid was washed with water until neutral pH followed by acetone, and dried. These samples are denoted CST- $R$  ( $0 \leq R \leq 1$ ), Table 1. The pure carbon material was prepared in the same way with  $R = 1$  (CT-1). For comparison, a silica impregnated with TsOH and heated at 160 °C (not thermally treated under N<sub>2</sub>) was prepared (CST-nc/a). A CST sample carbonized under N<sub>2</sub> at 600 °C for 1 h was also prepared (CST-0-600).

The stability of the materials was evaluated by performing pre-treatments of the solids (10 g<sub>solid</sub> dm<sup>−3</sup>) in ethanol (ET) at 110 °C or water (WT) at 170 °C, for 24 h. The solids were subsequently washed with ethanol (for ET), or water and then ethanol (for WT); all solids were dried at 85 °C. The resulting solids are denoted sample name-ET or -WT.

For comparative purposes, catalytic tests were performed by using the cation-exchange resin Amberlyst-15, a macroreticular styrene-divinylbenzene copolymer that bears benzenesulfonic acid groups and nanocrystalline beta zeolite in the protonated form (H-beta). Prior to use, the commercial Amberlyst-15 (FlukaChemika, in the form of beads) was ground and sieved to give a very fine powder. H-beta was prepared by calcination of commercial ammonium-form beta zeolite powder (NH<sub>4</sub>BEA, Zeolyst, CP814; crystallites with size of *ca.* 20–30 nm) at 550 °C for 10 h with a ramp rate of 1 °C min<sup>−1</sup> in static air.

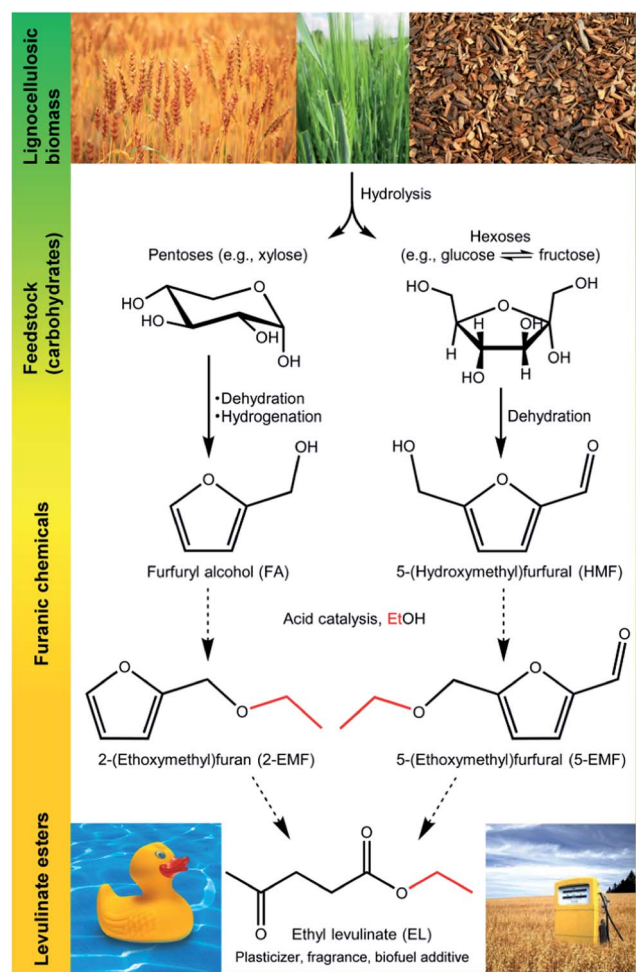


Fig. 1 Carbohydrate biomass conversion to useful bio products.



**Table 1** Preparation conditions, chemical and textural characteristics of the carbon and carbon–silica composite materials

Sample	$R^a$	$T^b$ (°C)	$C^c$ (wt%)	$S$ content <sup>c</sup> (mmol g <sup>-1</sup> )	Acid sites <sup>d</sup> (mmol g <sup>-1</sup> )	$A_{\text{BET}}^e$ (m <sup>2</sup> g <sup>-1</sup> )	$V_{\text{mp}}^f$ (cm <sup>3</sup> g <sup>-1</sup> )
CST-0	0	250	34.0	2.1	0.6	319	0.11
CST-0.1	0.1	250	26.6	1.6	0.7	331	0.09
CST-0.4	0.4	250	28.7	1.6	1.1	268	0.08
CST-1	1.0	250	26.1	1.7	1.6	237	0.05
CST-0-600	0	600	28.8	0.9	0.1	n.d.	n.d.
CT-1	1.0	250	47.7	2.9	2.8	9	—

<sup>a</sup> Mass of chemical activating agent/mass of carbon precursor. <sup>b</sup> Temperature of the carbonization or activation step. <sup>c</sup> Carbon and sulfur contents determined by CHNS elemental analysis. <sup>d</sup> Amount of acid sites determined by acid–base titration. <sup>e</sup> BET surface area. <sup>f</sup> Micropore volume.

### Characterization

The carbon and sulfur contents of the samples were determined by elemental analysis with a TruSpec 630 elemental analyzer. Powder X-ray diffraction (XRD) patterns were measured on a PANalytical Empyrean diffractometer at 45 kV and 40 mA, from 5 to 90° (2 $\theta$ ), with a step size of 0.08° and time per step of 400 s, using Cu K $\alpha$  radiation ( $\lambda$  = 0.1541 nm). FT-IR spectra were recorded on a Bruker Tensor 27 spectrometer using pellets of the sample mixed with KBr (400–4000 cm<sup>-1</sup>, 256 scans, 4 cm<sup>-1</sup> resolution). Raman measurements were carried out on a JobinYvon T64000 spectrometer (laser  $\lambda$ : 532 nm). X-ray photoelectron spectroscopy (XPS) analysis was performed on a K-Alpha system from Thermo Scientific, equipped with a monochromatic Al K $\alpha$  source (1486.6 eV), and operating in constant analyzer energy (CAE) mode with a pass energy of 200 and 50 eV for survey and high resolution spectra, respectively. A spot size diameter of about 400  $\mu$ m was adopted. Transmission electron microscopy (TEM) and high resolution TEM (HRTEM) images were recorded with Philips CM200 and JEOL 2200FS microscopes, respectively, at 200 kV. Nitrogen adsorption isotherms at –196 °C were measured with a Micromeritics Gemini 2380, after degassing of the samples at 120 °C overnight. The surface areas were calculated with the Brunauer–Emmett–Teller (BET) equation and the micropore volumes were calculated using the  $\alpha_s$  method, using standard data for N<sub>2</sub> adsorption on non-porous carbon. Thermogravimetric analyses (TGA) were performed from room temperature to 700 °C, with a heating rate of 5 °C min<sup>-1</sup>, under air flow on a Shimadzu TGA-50. The total acid sites content was determined by acid–base titration: the sample (0.1–0.2 g) was stirred at room temperature for 24 h in 20 mL of 0.1 M NaCl, and then titrated with 0.01 M NaOH. The acid strength of the solids was evaluated by <sup>31</sup>P MAS NMR of chemically adsorbed triethylphosphine oxide (TEPO). The adsorption of TEPO was performed as follows: 0.1 g of solid was dehydrated at 110–120 °C under vacuum. 0.015 g of TEPO dissolved in 5 mL of anhydrous *n*-pentane was added to the solid, and the mixture was stirred for 30 min under nitrogen, and then dried at 50 °C under vacuum. Solid-state NMR experiments were acquired on a Bruker Avance III 400 spectrometer using a 4 mm double resonance probe operating at a B0 field of 9.4 T (400 MHz) with a <sup>31</sup>P Larmor frequency of 161.9 MHz. <sup>31</sup>P {<sup>1</sup>H} MAS NMR spectra were recorded using a rotation speed of 12 kHz, a single excitation pulse width of 1.9  $\mu$ s, employing a

radio-frequency field strength of 56 kHz (60° flip angle) and 15 s recycle delay. TPPM-15 scheme was used for <sup>1</sup>H heteronuclear decoupling.

### Catalytic tests

The batch catalytic experiments were performed in tubular glass reactors with pear-shaped bottoms and equipped with an appropriate PTFE-coated magnetic stirring bar and a valve. In a typical procedure, 0.33 M 5-(hydroxymethyl)-2-furfural (HMF, Aldrich, 99%) or furfuryl alcohol (FA, Aldrich, 99%), powdered catalyst (loading of up to 10 g<sub>cat</sub> dm<sup>-3</sup>), and 1 mL of ethanol (Scharlau, 99.9%) were added to the reactor at 110 °C. The reaction of fructose (0.33 M) in the presence of the catalyst (10 g<sub>cat</sub> dm<sup>-3</sup>) was carried out using a water–ethanol (3 : 7 v/v ratio) solvent mixture, in the temperature range 110–170 °C. The reaction mixtures were heated with a thermostatically controlled oil bath, under continuous magnetic stirring at 1000 rpm. Zero time (the instant the reaction began) was taken to be the instant the micro-reactor was immersed in the oil bath. The heating time to reach 110–140 °C was 3–4 min, and to reach 170 °C, was 6 min. The initial reaction rates are based on conversion at 30 min reaction. The CST-1 catalyst was separated, after a 4 h batch run by centrifugation, washed with ethanol and then water, and subsequently treated with H<sub>2</sub>SO<sub>4</sub> (0.2 M) for 4 h at 30 °C. The catalyst was subsequently washed with water until the pH was neutral and dried at 85 °C overnight.

The evolution of the catalytic reactions was monitored by GC (for quantification of bioEs and FA) and HPLC (for quantification of HMF and fructose). Prior to sampling, the reactors were cooled to ambient temperature before opening and work-up procedures, and no pressure-release was verified. The GC analyses were carried out using a Varian 3800 equipped with a capillary column (Chrompack, CP-SIL 5CB, 50 m  $\times$  0.32 mm  $\times$  0.5  $\mu$ m) and a flame ionisation detector, using H<sub>2</sub> as carrier gas. Authentic samples of the substrates were used as standards, and calibration curves were measured for quantification. The HPLC analyses were carried out using a Knauer Smartline HPLC Pump 100 and a Shodex SH1011 H<sup>+</sup> 300 mm  $\times$  8 mm (i.d.) ion exchange column (Showa Denko America, Inc., New York), coupled to a Knauer Smartline UV detector 2520 (254 nm for HMF), and a Knauer Smartline 2300 differential refractive index detector (for fructose); the mobile phase was 0.005 M aq. H<sub>2</sub>SO<sub>4</sub>





at a flow rate of  $0.8 \text{ mL min}^{-1}$ , and the column temperature was  $50^\circ\text{C}$ . The identification of the reaction products was accomplished by GC-MS using a Trace GC 2000 Series (Thermo Quest CE Instruments) – DSQ II (Thermo Scientific), equipped with a capillary column (DB-5 MS,  $30 \text{ m} \times 0.25 \text{ mm} \times 0.25 \mu\text{m}$ ), using He as carrier gas. Individual experiments were performed for a given reaction time and the presented results are the mean values of at least two replicates.

The substrate (Sub) conversion (%) at reaction time  $t$  was calculated using the formula:  $100 \times [(\text{initial concentration of Sub}) - (\text{concentration of Sub at time } t)] / (\text{initial concentration of Sub})$ . The yield of product (Pro) (%) at reaction time  $t$  was calculated using the formula:  $100 \times [(\text{concentration of Pro at time } t) / (\text{initial concentration of Sub})]$ .

The bioEs products were EL (ethyl levulinate) and 5EMF (5-(ethoxymethyl)-furfural) for fructose and HMF as substrates, and EL and 2EMF (2-(ethoxymethyl)-furan) for FA as substrate.

## Results and discussion

### Effect of the synthesis conditions on the properties of the materials

Carbon (CT-1) and carbon-silica composites (CST-R) were prepared by chemical activation of *p*-toluenesulfonic acid (TsOH) with sulfuric acid at  $250^\circ\text{C}$ . In particular, the CST-R materials consist of a carbon film deposited on fumed silica particles of *ca.* 7–10 nm (Fig. 2) and were synthesized using different  $\text{H}_2\text{SO}_4$ /organic precursor mass ratios ( $R$ ). For comparison, a related material was prepared by carbonization at  $600^\circ\text{C}$  to give CST-0-600.

The carbon component of the composites accounts for *ca.* 40% of the materials weight, as ascertained by TGA (Fig. S1, ESI†). The sulfur content of the final solids depends on the synthesis conditions (Table 1). Carbonization at  $600^\circ\text{C}$  results

in a material with low S content (CST-0-600) in comparison to materials synthesized at  $250^\circ\text{C}$ . The chemically activated CST composites have similar S contents, which correlates with the similar amount of carbon precursor used for their syntheses, and does not correlate with  $R$ . These results suggest that the S groups in the final solids derive essentially from the carbon precursor. In fact, the amount of S was higher when no chemical activating agent was added (CST-0). The amount of sulfur and acid sites per mass of material is higher for CT-1 than CST-1 due to the absence of the silica component on the former. In fact, if we only take into account the mass of carbon component of the materials for calculating the S and acid sites content, higher values are obtained for CST-1 with respect to CT-1. Hence, a more sulfur-enriched carbon is produced *via* the coating approach, as a result of the dispersion of the carbon over the silica. It is possible that reactions such as condensation between the silica surface (*e.g.* silanol groups) and the organic (*e.g.*  $\text{SO}_3\text{H}$  groups) take place during carbonization, leading to a strong interaction between carbon and silica.<sup>61</sup>

The surface texture of the carbon and composite materials is very different (Table 1, Fig. S2, ESI†). The CT-1 material has very low specific surface area, which is not much higher than those of carbons produced by incomplete carbonization of carbohydrates and other organic molecules.<sup>4,14,24</sup> Coating the silica particles with the carbon film allows the control of the catalyst morphology and, additionally, of the surface area. The silica support is a high surface area non-porous solid ( $A_{\text{BET}} = 346 \text{ m}^2 \text{ g}^{-1}$ , Fig. S3, ESI†). The composites also have relatively high surface areas, and their surface texture depends on  $R$ . For  $R = 0$  (CST-0) a highly microporous carbon coating was formed, whereas the micropore volume decreases with increasing  $R$ . For CST-0, the isotherm is close to type I, typical of microporous solids, and the absence of hysteresis indicates that the sample does not have mesopores. The amount adsorbed at intermediate and high  $p/p^0$  tends to increase as  $R$  increases. Moreover, for CST-0.4 and CST-1, the isotherms exhibit H3 hysteresis cycles, indicating the presence of slit-like shaped mesopores on the materials (Fig. S2, ESI†). The hysteresis cycle is larger over a wider range of  $p/p^0$  for CST-1 compared to CST-0.4, and is associated to higher amounts of  $\text{N}_2$  adsorbed, which suggests that CST-1 has more mesoporosity than CST-0.4. These results suggest that some micropores are converted into mesopores by increasing  $R$ . The creation and enlargement of pores is an intrinsic characteristic of chemical activation processes,<sup>29,30</sup> and it is caused by the chemical attack on the carbon matrix.

The powder X-ray diffractograms of the materials show a broad peak centered at  $22^\circ$  ( $2\theta$ ), corresponding to diffraction by (002) graphitic planes (Fig. S4, ESI†), that indicates the presence of amorphous carbon on the solids with a highly disordered arrangement of small carbon sheets.<sup>12,22</sup> The Raman spectra (Fig. S5, ESI†) exhibit broad bands at  $1355$  and  $1855 \text{ cm}^{-1}$  ascribed to the carbon A1g and E2g vibration modes, confirming the highly disordered structure of the carbon.<sup>11</sup>

Assessment of the type and relative amounts of the surface functional groups in the materials was made by combining FT-IR, high resolution XPS and solid state NMR techniques. For

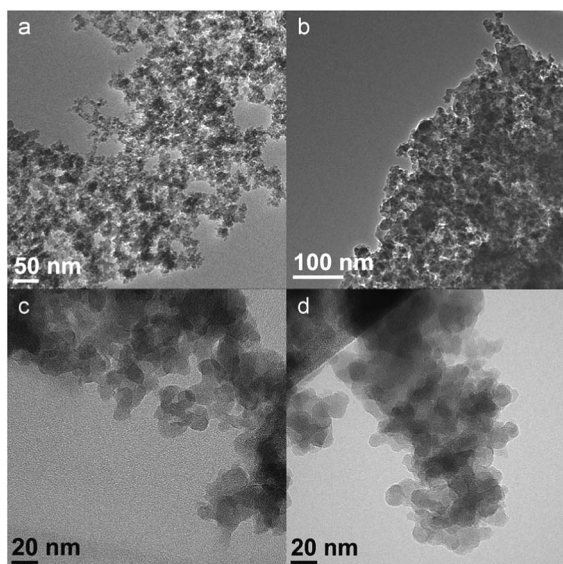


Fig. 2 TEM images of the (a) silica support, (b) CST-1 composite, and HRTEM images of (c) CST-1 and (d) CST-0.



comparison, a CST composite prepared with  $R = 0$  and without thermal treatment under  $N_2$  (CST-nc/a) was also investigated.

The FT-IR spectra of the composites exhibit bands at 468, 808, 970 and  $1101\text{ cm}^{-1}$  associated to the silica component of the materials (Fig. S6, ESI†). The spectrum of CST-nc/a (Fig. 3f), in addition to the bands of the silica component, shows bands typical of aromatic organic compounds.<sup>62</sup> In particular, the bands at 686 and  $570\text{ cm}^{-1}$  are attributed to aromatic C–H bending and out-of-plane ring bending, respectively. These bands are still visible in the spectrum of CST-0 (Fig. 3e), although with relatively low intensity, suggesting that CST-0 still contains some non-carbonized precursor. On the contrary, these bands are not observed in the spectra of the chemically activated materials and CST-0-600 sample (Fig. S6, ESI†) indicating that pyrolysis was more extensive for these materials, which reflects the promoting role of the activating agent on the transformation of the precursor into carbon. The  $^1\text{H}$ - $^{13}\text{C}$  CP MAS NMR data is in agreement with these results (Fig. S7 and S8, ESI†). The bands at 1175 and  $1028\text{ cm}^{-1}$  in the CT-1 spectrum are related to the  $\text{SO}_3\text{H}$  groups,<sup>11,12</sup> while those at 1715, 1771 and  $1389\text{ cm}^{-1}$  are ascribed to ketones, carboxylic acids and hydroxyl groups respectively (Fig. 3a). Moreover, the band at  $ca. 620\text{ cm}^{-1}$  has been attributed to the stretching of C–S bonds.<sup>12</sup>

These bands are difficult to see in the spectra of the composites due to the comparatively high intensity of the bands associated to the silica. Nevertheless, for the composites, those assigned to COOH and C=O groups become more intense as  $R$  increases, suggesting an increase in the degree of the carbon oxidation (Fig. 3b–d).

The S 2p X-ray photoelectron spectra of the composites exhibit 2 contributions, whose relative intensity depends on  $R$  (Fig. 4). The band at 169 eV is attributed to sulfur in  $\text{SO}_3\text{H}$  groups and the band at 164 eV indicates the presence of sulfur in SH groups.<sup>63,64</sup> The SH/ $\text{SO}_3\text{H}$  ratio is 0.7, 1.0, 0.6 and 0.2 for

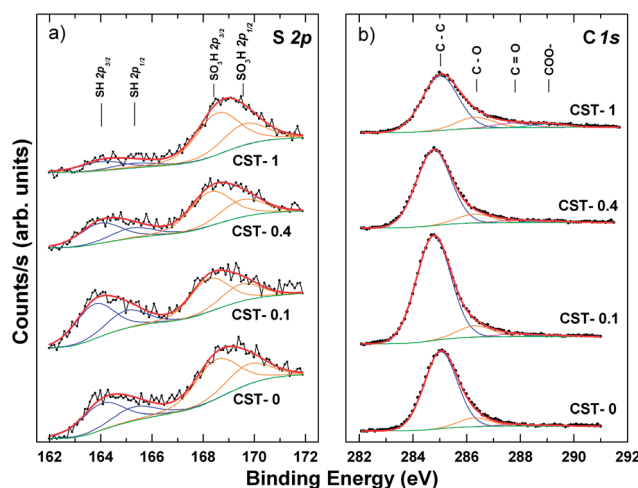


Fig. 4 Deconvoluted (a) S 2p and (b) C 1s X-ray photoelectron spectra of the CST- $R$  composites.

$R = 0, 0.1, 0.4$  and  $1.0$ , respectively (Table S1, ESI†). For CST-0 and CST-0.1, 40–50% of the surface sulfonic acid groups are reduced to thiol groups. The relative amount of SH groups decreases as  $R$  increases, probably caused by the progressively stronger oxidizing conditions during thermal treatment under nitrogen. Hence, for CST-1 most of the sulfur corresponds to sulfonic acid groups (>80%). Differences in the C 1s profiles are also observed for different  $R$ . Deconvolution of the C 1s bands showed four contributions: a main contribution at  $ca. 285\text{ eV}$  attributed to carbon–carbon bonding, and three other contributions at higher binding energies corresponding to carbon atoms bonded to oxygen in different surface functionalities. The C–S contribution cannot be distinguished from the C–C band. The bands at 286.3 eV, 287.7 eV and 289.1 eV are attributed to C–O bonds (such as in hydroxyl groups), carbonyl and carboxylic acid groups, respectively.<sup>65,66</sup> The ratio between the percentages corresponding to C–C and (C–O, C=O or COO–), in general decreases as  $R$  increases, reflecting an increase in the degree of surface carbon oxidation (Table S2†). The percentage of C–O bonding is much lower for CST-0 and CST-0.1 compared to CST-1.

An assessment of the relative amount of acid sites and their acid strengths was obtained by  $^{31}\text{P}$  MAS NMR spectroscopy of adsorbed TEPO as a base probe molecule (Fig. 5; Table S3 of ESI† for the deconvolution fitting data). The spectra show distinct profiles for each material, indicating that the acid properties are significantly influenced by the preparation conditions. The CST materials show essentially six resonances with a range of chemical shift values spanning from  $ca. 50$  to  $100\text{ ppm}$ . The interaction of TEPO with acid sites of increasing strength causes the  $^{31}\text{P}$  resonance to shift downfield, *i.e.*, stronger acid sites lead to higher chemical shifts.<sup>67,68</sup> Therefore, the materials contain acidity ranging from weak ( $\sim 50$ – $60\text{ ppm}$ ), medium ( $\sim 70\text{ ppm}$ ), strong ( $\sim 80\text{ ppm}$ ) to very strong ( $90$ – $100\text{ ppm}$ ). Moreover, the  $^{31}\text{P}$  spectra and deconvolution values for the CST-0, CST-0.1, CST-0.4 and CST-1 materials indicate that the chemical shift values and peak intensities of certain

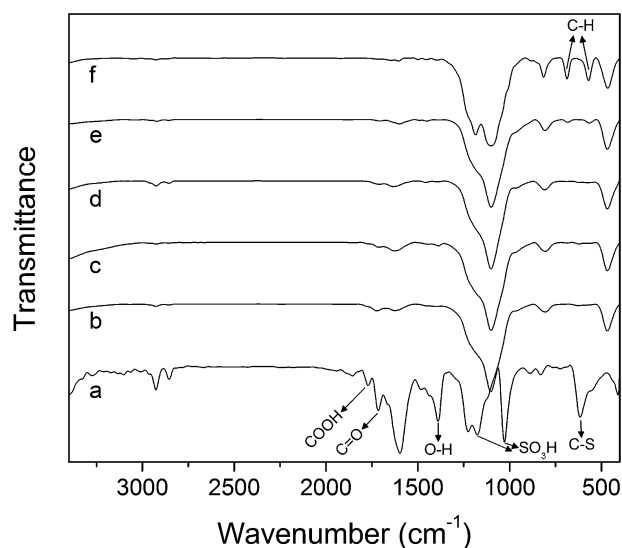


Fig. 3 FT-IR spectra of (a) CT-1, (b) CST-1, (c) CST-0.4, (d) CST-0.1, (e) CST-0 and (f) CST-nc/a.



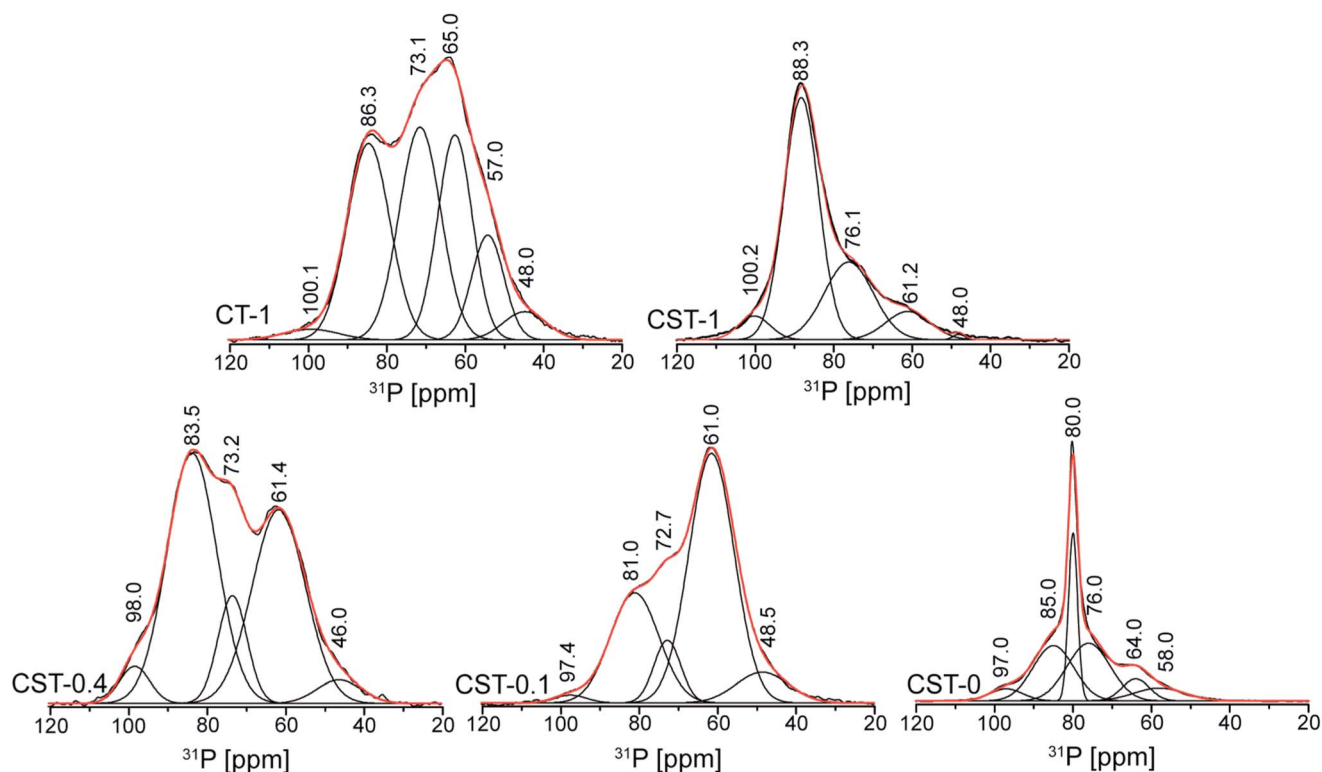


Fig. 5  $^1\text{H}$ -decoupled  $^{31}\text{P}$  MAS NMR spectra and spectral deconvolutions of the CT-1 and CST-R materials after adsorption of TEPO.

resonances change across the series. For example, in CST-0.1, the strongest acid site is *ca.* 97 ppm, and the most abundant acid site is at 61 ppm with a percentage area of 56%. Comparing these values with those in the CST-1 material, the strongest acid site is *ca.* 100 ppm and its most abundant acid site is 88 ppm. This means that not only does the overall acidity become stronger, but also the amount of stronger acid sites increases as a function of increasing *R* values. The resonance at *ca.* 48 ppm is ascribed to physisorbed TEPO.<sup>69</sup> According to the FT-IR and XPS results, the CST-materials have different types of acid sites with varied strength. Therefore, the resonances at *ca.* 61 and 72 ppm are probably associated with the relatively weaker OH and COOH acid groups, respectively, and those at higher chemical shifts correspond to the stronger SO<sub>3</sub>H groups.<sup>10</sup> The resonance at *ca.* 97–100 ppm may be due to TEPO interacting with sulfuric ester groups, since these groups are expected to be stronger than SO<sub>3</sub>H. However, sulfuric esters could not be identified by FT-IR or XPS. On the basis of the FT-IR,  $^{13}\text{C}$  NMR and  $^{31}\text{P}$  NMR data for CST-0, the narrow and intense peak at *ca.* 80 ppm is ascribed to TEPO interacting with the carbon precursor. The CST-1 material not only possesses the strongest acidity, but also the greatest amount of strong acid sites compared to the other composites. By comparing the  $^{31}\text{P}$  NMR spectra of CT-1 and CST-1, it seems that combination of the carbon with the silica generates a higher relative amount of stronger acid sites, *i.e.*, a stronger solid acid. The reason for this is not clear, but it may be related with interactions established between the carbon and silica. Our catalysts have a wider distribution of acid strengths

than Amberlyst-15 (displays a single resonance at 90.5 ppm),<sup>10</sup> and some stronger acid sites.

The acid sites content measured by titration is the total amount of acid sites of the sample, which includes sulfonic acid, carboxylic acid and hydroxyl groups. The total amount of acid sites is lower than the sulfur content of the corresponding sample (Table 1). On the one hand, some of the sulfur is in the form of SH groups. On the other hand, since the sulfur of the materials derives from the precursor, part of it is probably located in the bulk and not at the surface. For the chemically activated composites, the difference between the S and acid sites contents decreases as *R* increases, which can be explained by the increase of the acidic S-containing functionalities and other acid surface groups (carboxylic acids, hydroxyls) found by XPS analysis. Carbonization at 600 °C led to very low quantity of acid sites (CST-0-600, Table 1), as most of the surface sulfonic acid groups of the precursor were decomposed at this temperature, which is disadvantageous for acid catalysis.

### Catalytic studies

**Reactions of 5-hydroxymethyl-2-furaldehyde (HMF) and fructose to bioEs.** The effect of the synthesis activation conditions on the catalytic activity was first evaluated by performing the reaction of HMF with ethanol (Fig. 1) in the presence of the composite materials, using the same catalyst loading (10 g<sub>cat</sub> dm<sup>-3</sup>), at 110 °C (Fig. 6 and 7, Table 2). This type of comparison is interesting for practical purposes. The activated composite catalysts gave 95–97% of bioEs yield (bioEs stands



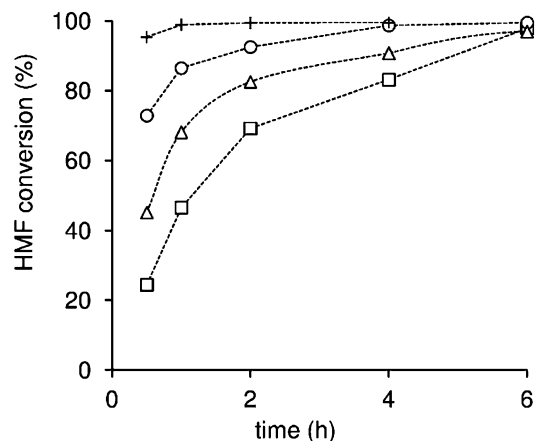


Fig. 6 Kinetic profiles of the reaction of HMF in the presence of CST-0.1 (□), CST-0.4 (Δ) and CST-1 (O) at 110 °C, or in the presence of CST-1 at 140 °C (+). Reaction conditions:  $[HMF]_0 = 0.33$  M, catalyst loading =  $10 \text{ g}_{\text{cat}} \text{ dm}^{-3}$  (the dashed lines are guides to the eye).

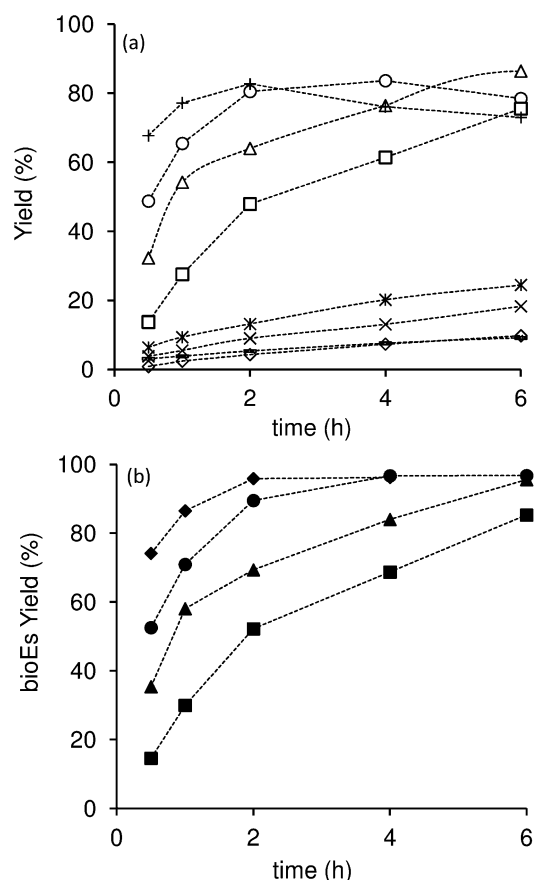


Fig. 7 Dependency of the yields of (a) 5EMF (+, o, Δ, □) and EL (\*, -, x, ◇), or (b) bioEs (◆, ●, ▲, ■) on the time of the reaction of HMF in the presence of CST-0.1 (□, ◇, ■), CST-0.4 (Δ, -, ▲) or CST-1 (o, x, ●) at 110 °C, or in the presence of CST-1 at 140 °C (+, \*, ◆). Reaction conditions:  $[HMF]_0 = 0.33$  M; catalyst loading =  $10 \text{ g}_{\text{cat}} \text{ dm}^{-3}$  (the dashed lines are guides to the eye).

for 5EMF and EL) at >99% conversion, although at different reaction times. The reaction in the presence of the silica, on the other hand, was very sluggish, with 2% bioEs yield reached at

Table 2 Reaction of HMF to bioEs in the presence of the CST catalysts<sup>a</sup>

Catalyst	Time (h)	Conversion (%)	Yields of bioEs products (%)		
			5EMF	EL	bioEs
CST-0.1	4/16	83/99	62/83	7/13	69/96
CST-0.4	4/6	91/97	76/86	8/9	84/95
CST-1 (run 1)	4	99	84	13	97
CST-1 (run 2)	4	95	86	7	93
CST-1 (run 3)	4	92	83	6	91
CST-1-WT	4	98	85	10	95
CST-1-ET	4	99	81	13	94
CST-1-ET(2)	4	99	80	15	95
CST-0	4	96	75	15	90
CST-0-ET	4	72	57	5	62

<sup>a</sup> Reaction conditions:  $[HMF]_0 = 0.33$  M; catalyst loading =  $10 \text{ g}_{\text{cat}} \text{ dm}^{-3}$ , 110 °C.

24 h and 25% conversion, confirming that the functionalized carbon is the active component of the composites. Increasing the reaction temperature to 140 °C led to considerably faster initial reaction for CST-1 (Fig. 6), with 96% of bioEs yield at 100% conversion being reached within 2 h (Fig. 7). However, to facilitate comparisons between the catalysts, a lower reaction temperature was used. 5EMF was the main product detected, which was formed in similar maximum yields of 83–86% but at 4, 6 and 16 h of reaction for CST-1, CST-0.4 and CST-0.1, respectively. After reaching a maximum, the 5EMF yields tended to decrease with the concomitant increase in EL yields (shown in Fig. 7 for CST-1), which is consistent with 5EMF being an intermediate of the conversion of HMF to EL.<sup>46,53,54</sup>

The initial reaction rates were 16, 30 and  $48 \text{ mmol g}_{\text{cat}}^{-1} \text{ h}^{-1}$  for CST-0.1, CST-0.4 and CST-1, respectively. The higher reaction rate observed for CST-1 was accompanied by the higher initial bioEs yield at 30 min. Therefore, the CST-1 material exhibits better catalytic performance than the other composites. Moreover, the catalytic activity increases in the following order CST-0.1 < CST-0.4 < CST-1. On the basis of these results, increasing *R* of the synthesis leads to higher reaction rates and bioEs yields, as a result of enhanced amount and strength of the acid sites.

To get clearer insights into the intrinsic activity of the catalysts, the reaction of HMF was performed using the same initial molar ratio between HMF and the total acid sites of the material for all catalysts ( $HMF/AS = 50$ , AS denotes acid sites) (Fig. 8, S9 and S10†). The initial reaction rates were 25, 40 and  $60 \text{ mol mol}_{\text{AS}}^{-1} \text{ h}^{-1}$ , and the initial bioEs yields at 30 min were 15, 28 and 43% for CST-0.1, CST-0.4 and CST-1, respectively. The trends are similar to those obtained for the same catalyst loading. These results indicate that, besides the amount of acid sites, the strength of the acid sites play an important role in the conversion of HMF, with stronger acid sites favouring the overall reaction.

The carbon catalyst CT-1 is less active than the related composite CST-1 (Fig. 8). For CT-1, the initial reaction rate was  $40 \text{ mol mol}_{\text{AS}}^{-1} \text{ h}^{-1}$ , and the total bioEs yields at 30 min





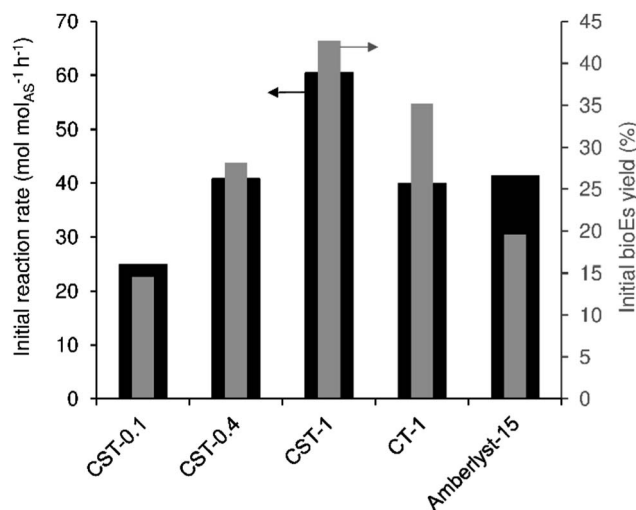


Fig. 8 Initial reaction rate of HMF and bioEs yields at 30 min for the prepared catalysts and Amberlyst-15 using the same initial molar ratio of HMF/AS = 50 (AS = acid sites). Reaction conditions: [HMF]<sub>0</sub> = 0.33 M, 110 °C.

reaction was 35% which increased to 73% at 96% conversion. Considering the high acid sites content and low surface area of CT-1, a significant portion of its acid sites is most likely located inside the carbon matrix and thus may be strongly hindered or even inaccessible for the catalytic reaction. Furthermore, the relative proportion of acid sites of moderate or low strength is higher for CT-1 than for CST-1, as determined by <sup>31</sup>P NMR of adsorbed TEPO. These factors can explain the poorer catalytic performance of CT-1.

The performances of our catalysts were compared with that of the reference commercial acid-resin Amberlyst-15 (Fig. 8), which has high content of strong sulfonic acid groups (4.3 mmol g<sup>-1</sup>, as measured by acid–base titration). This solid acid has shown excellent activity in the reaction of HMF to bioEs and several other acid-catalyzed reactions. The initial reaction rate for Amberlyst-15 was 41 mol mol<sup>-1</sup> s<sup>-1</sup>, which is similar to that for CST-0.4 and lower than that for CST-1. The acid resin also led to lower bioEs yield at 30 min compared to these catalysts. Furthermore, for Amberlyst-15 the bioEs yield dropped at high HMF conversion (82% yield at 92% conversion dropped to 75% at 99% conversion (Fig. S9 and S10<sup>†</sup>)), while for CST-1 the yield increased continuously, reaching 97% at 100% conversion. Therefore, CST-1 possesses superior intrinsic activity for the conversion of HMF to bioEs than Amberlyst-15, despite having a much lower amount of acid sites of comparable strength. Considering the low surface area of the polymeric resin and its high sulfonic acid groups content, the acid sites density for the resin catalyst is probably much higher than the estimated maximum number of HMF molecules per unit of surface area (*ca.* 3 molecules nm<sup>-2</sup>),<sup>70</sup> even after it swells. It is worth mentioning that in order to enhance the active site accessibility, the acid resin (commercialized in the form of beads) was ground prior to use, to give a very fine powder with particles of a few hundreds of nanometers (Fig. S11<sup>†</sup>). Hence, one may expect steric hindrance at the vicinity of a significant

fraction of the acid sites of the resin catalyst that can affect the overall reaction of HMF. Additionally, very high acid sites density may favour undesirable consecutive reactions, decreasing the selectivity of the catalyst.

Table S4<sup>†</sup> compares the catalytic results for CST-1 with those reported in the literature for other catalysts. Some clear and fair comparisons of the catalysts can be made (tested under similar reaction conditions). Mesoporous aluminosilicates of the type Al-TUD-1 (ref. 58) and sulfonated partially reduced graphene oxide (S-RGO)<sup>10</sup> were previously tested as catalysts in the same reaction, under similar conditions to those used in the present work. In comparison with the aluminosilicates, CST-1 exhibits higher catalytic activity and leads to higher bioEs yields in shorter reaction time, which may be partly due to its stronger acidity and higher amount of acid sites. The catalytic performance of CST-1 is comparable to that of S-RGO, and superior to those of sulfonated carbon nanotubes and carbon black.<sup>10</sup> In comparison to those carbon catalysts, the materials tested here have advantages, including the fact that their preparation involves less drastic acidic conditions.

We further compared the catalytic performance of CST-1 to nanocrystalline zeolite H-beta; the latter led to much slower conversion of HMF to bioEs than CST-1 (Table S4<sup>†</sup>). Conversion at 4 h was 99% and 67%, and bioEs yield was 97% and 56% for CST-1 and H-beta, respectively; in the case of the zeolite the EL yield was less than 1%. The catalytic performance of CST-1 remained superior to the classical zeolite and acid resin even under much more concentrated reaction conditions, *i.e.* a greater initial amount of HMF (*ca.* 3.9 times greater than the typical conditions) and less solvent (half the amount), Fig. S12 and Table S4<sup>†</sup>; the conversions and bioEs yields at 4 h reaction were similar to those obtained using less concentrated conditions. Hence, it may be possible to further optimise the reaction conditions to achieve higher production yields of bioEs.

The CST-1 material was also tested as a catalyst in the integrated conversion of fructose to bioEs (Fig. 1). The conversion of fructose in a water–ethanol mixture (3 : 7, v/v; fructose was completely dissolved at room temperature) increased with the increase of the reaction temperature in the range 110–170 °C (Table 3). The main products identified were HMF, 5EMF and EL that were formed with yields of 13, 38 and 15%, respectively, at 100% conversion at 170 °C. Without adding a catalyst the conversion of fructose was 24% after 24 h reaction at 170 °C, and the HMF, 5EMF and levulinic acid (LA) yields were 14, 5 and <1%, respectively. These results are somewhat in agreement with those reported in the literature that suggest the reaction of fructose may be to a certain extent autocatalytic.<sup>71</sup> The reaction of fructose using solely water as solvent at 170 °C led to relatively low yields of HMF and LA at 95% conversion (Table 3). Hence, the conversion of fructose using ethanol as co-solvent is more selective towards valuable bio products in comparison to the aqueous phase system. These results are in agreement with those in the literature indicating that in alcohol media the formation of humins is avoided, leading to cleaner reaction mixtures.<sup>45,54,72,73</sup> Using this approach the product separation and purification processes may be facilitated. Comparison of the catalytic performance of CST-1 with that of Amberlyst-15 in





Table 3 Reaction of fructose in the presence of CST-1<sup>a</sup>

Solvent	Reaction conditions <sup>a</sup>		Conv. <sup>b</sup> (%)	Product yield (%)			
	<i>T</i> (°C)	<i>t</i> (h)		HMF	LA	5EMF	EL
Ethanol–water	110	4/24	12/50	9/26	—	—/5	—/1
Ethanol–water	140	4/24	49/95	25/28	—	2/27	(<1)/7
Ethanol–water	170	1/4/24	78/100/100	43/32/13	<1/<1/5	7/24/38	1/5/15
H <sub>2</sub> O	170	24	95	9	20	—	—

<sup>a</sup> Reaction conditions: initial molar concentration of fructose = 0.33 M, catalyst load = 10 g<sub>cat</sub> dm<sup>-3</sup>, *T* = reaction temperature (°C), *t* = time of reaction (h). <sup>b</sup> Fructose conversion.

the reaction of fructose at 110 °C (the maximum operation temperature recommended is 120 °C), indicated poorer products selectivity at similar conversion in the case of the acid resin catalyst: 9% HMF yield and no bioEs were detected at 44% fructose conversion, whereas CST-1 led to 26% HMF and 6% bioEs yield at 50% conversion.

**Reaction of furfuryl alcohol to bioEs.** The versatility of the catalysts was further investigated for the reaction of furfuryl alcohol (FA) with ethanol, at 110 °C (Fig. 9, Table S5†). The complete conversion of FA was reached at 2 h for CST-0.1 and 30 min for the other catalysts. The main initial product was 2EMF, formed in a maximum yield of ca. 48% at 30 min reaction for CST-0.4. The consumption of 2EMF with time was accompanied by the formation of EL in high yields (82–86%) within 16–24 h of reaction. Hence, FA is much more reactive than HMF for producing EL under similar reaction conditions, in agreement with the data reported in the literature for other catalysts.<sup>58</sup> The kinetic features observed are consistent with the intermediate formation of at least 2EMF in the conversion of FA to EL.<sup>56,59,74</sup>

The increase of the reaction temperature to 140 °C in the presence of CST-1 led to the same maximum EL yield of ca. 81% although reached within 6 h instead of 16 h at 110 °C. The trends in the catalytic performance of the materials are similar to those observed for the reaction of HMF, but with less differences between the several catalysts. These trends are therefore explained by the differences in the amount and strength of the acid sites of the catalysts, in parallel to that discussed above for the HMF conversion.

The reaction of FA and its intermediates to EL is gradually more favoured as the acidity of the CST material increases, with CST-1 being the most active catalyst. CST-1 is also a more effective catalyst than its pure carbon analogue, as also found for the HMF reaction. Therefore, the combination of the carbon with a high surface area silica results in more effective catalysts for both the HMF and FA conversion. The CST-1 material is also a considerably better catalyst than several other solid acids tested in the reaction of FA under similar conditions, namely mesoporous aluminosilicates and zeolites.<sup>59</sup>

**Stability of the catalysts under the reaction conditions.** Leaching or dissolution of sulfur-containing species into the reaction mixtures is frequently observed for catalysts with sulfonic acid groups, which can cause drastic losses of activity after just one catalytic cycle.<sup>10,20,24,25</sup> In carbon catalysts

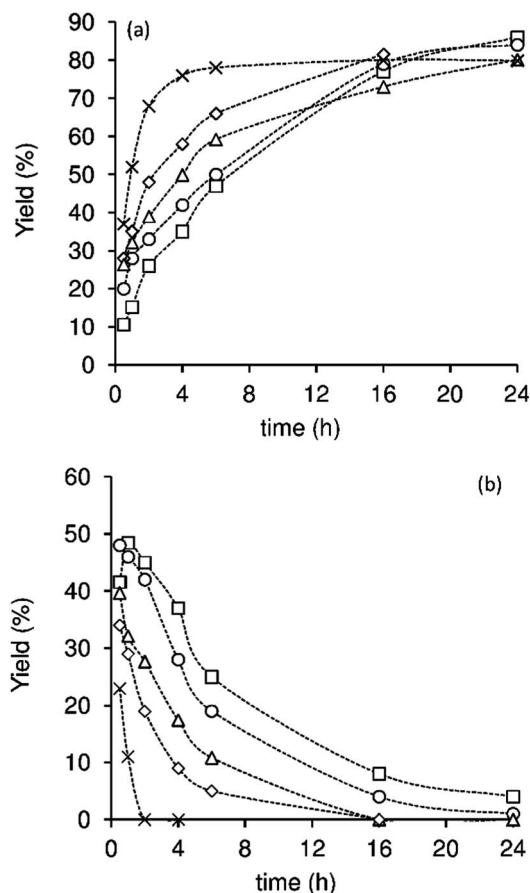


Fig. 9 Dependence of the yield of (a) EL and (b) 2EMF on the time of reaction of FA in the presence of CT-1 ( $\Delta$ ), CST-0.1 ( $\square$ ), CST-0.4 ( $\circ$ ) and CST-1 ( $\times$ ) at 110 °C, or in the presence of CST-1 ( $\times$ ) at 140 °C (lines are guides to the eye). Reaction conditions:  $[FA]_0 = 0.33$  M, catalyst loading = 10 g<sub>cat</sub> dm<sup>-3</sup>.

synthesized by thermal treatment of organic molecules at low temperatures it is usually attributed to the dissolution of non-carbonized organic sulfonated compounds. The stability of the materials in terms of SO<sub>3</sub>H leaching can be assessed by pre-treatment of the catalysts in the solvent, at the reaction temperature in the absence of the substrate. Therefore, our catalysts were pre-treated in ethanol at 110 °C for 24 h (ET) and water at 170 °C for 24 h (WT) in order to evaluate their stability.

The samples CST-1-ET and CST-1-WT contained the same amount of sulfur and acid sites as the original solid ( $1.7 \text{ mmol g}^{-1}$  and  $1.6 \text{ mmol g}^{-1}$ , respectively), indicating that loss of S-containing moieties did not occur. The stability was further confirmed by testing the pre-treated samples in the reaction of HMF (Table 2). Both pre-treated samples exhibited catalytic performance identical to that of CST-1. Indeed, after two consecutive treatments in ethanol, the resultant solid CST-1-ET(2) continued to show catalytic performance similar to CST-1. For the material prepared by thermal treatment at  $250^\circ\text{C}$  without the addition of the activating agent (CST-0), considerable drops in the amount of sulfur and acid sites occurred after the pre-treatments in ethanol or water. The CST-0-ET and CST-0-WT samples contained  $1.6 \text{ mmol g}^{-1}$  of sulfur and  $0.2 \text{ mmol g}^{-1}$  of acid sites, which corresponds to a 24% loss of sulfur and 66% loss of acid sites. As expected, these samples led to much lower HMF conversion and bioEs yields than the parent solid CST-0 (Table 2). Therefore, although CST-0 exhibited relatively high catalytic activity, its low stability limits its re-use and its application.

The FT-IR spectra of the CST-0-ET and CST-0-WT samples (Fig. S13, ESI†) lack the bands at  $686$  and  $570 \text{ cm}^{-1}$  that were found in the spectrum of CST-0 and assigned to non-carbonized organic precursor. Hence, the low stability of CST-0 can be attributed to the presence of a significant amount of non-carbonized carbon precursor on the material that is easily leached into the solvents under the reaction conditions used.

The CST-1 catalyst was recovered and reused in consecutive 4 h-batch runs. The conversion and bioEs yield dropped slightly from the first to the second run and afterwards remained similar. Based on the results of the reused solids,  $14.1 \text{ g bioEs per gram of catalyst}$  is obtainable after three runs. We have previously reported for powdered Amberlyst-15 tested in the same reaction (using similar conditions) that the recovered resin catalyst led to similar conversions of HMF for two runs, but with a very considerable decrease in bioEs yield from run 1 to run 2.<sup>10</sup>

## Conclusions

Carbon and carbon-silica composites containing  $\text{SO}_3\text{H}$  groups were synthesized by chemical activation of *p*-toluenesulfonic acid with  $\text{H}_2\text{SO}_4$  at  $250^\circ\text{C}$ . This procedure allows tuning the surface composition, texture and acid properties of the materials, leading simultaneously to solids that are stable towards leaching phenomena. By increasing the ratio (*R*) between the activating agent and the organic precursor, the amount and strength of the acid sites increase, and this is accompanied by the creation of mesoporosity, which enhances active sites accessibility.

The chemically activated composites are effective acid catalysts for the conversion of 5-hydroxymethyl-2-furaldehyde and furfuryl alcohol to furanic ethers and levulinate esters (bioEs), and the integrated conversion of fructose to bioEs. The much higher surface areas and strong acidity associated with the carbon-silica composites are favourable for the catalytic reactions, making them top candidates in relation to the carbon

material. For the composites, stronger acidity with increasing *R* was reflected in enhanced reaction rates and yields of the bio products.

This synthesis approach can be used to prepare functionalized carbon-based materials in controllable fashion for various applications, by using other carbon precursors, activating agents or mixtures of carbon precursors with different functionalities (to produce multifunctional materials).

## Acknowledgements

We are grateful to the Fundação para a Ciência e a Tecnologia (FCT) and FEDER for general funding, and to CICECO – FCOMP-01-0124-FEDER-037271 (FCT ref. PEst-CTM/LA0011/2013). The FCT and the European Union are acknowledged for grants to M.M.A. (SFRH/BPD/89068/2012), P.A.R. (SFRH/BPD/79910/2011) and P.N. (SFRH/BPD/73540/2010) cofunded by MCTES and the ESF through the program POPH of QREN. We acknowledge the Portuguese National NMR Network (RNRMN), supported with funds from the FCT. BP Amoco Chemical Company is acknowledged for sponsoring P.V.W.'s postdoc grant. L.M. thanks the FCT for the FCT Investigator consolidation grant IF/01401/2013.

## Notes and references

- 1 G. W. Huber, S. Iborra and A. Corma, *Chem. Rev.*, 2006, **106**, 4044–4098.
- 2 R. Rinaldi and F. Schüth, *Energy Environ. Sci.*, 2009, **2**, 610–626.
- 3 C.-H. Zhou, X. Xia, C.-X. Lin, D.-S. Tong and J. Beltramini, *Chem. Soc. Rev.*, 2011, **40**, 5588–5617.
- 4 K. Nakajima and M. Hara, *ACS Catal.*, 2012, **2**, 1296–1304.
- 5 M. Toda, A. Takagaki, M. Okamura, J. N. Kondo, S. Hayashi, K. Domen and M. Hara, *Nature*, 2005, **438**, 178.
- 6 M. Hara, T. Yoshida, A. Takagaki, J. N. Kondo, S. Hayashi and K. Domen, *Angew. Chem., Int. Ed.*, 2004, **43**, 2955–2958.
- 7 X. Wang, R. Liu, M. M. Waje, Z. Chen, Y. Yan, K. N. Bozhilov and P. Feng, *Chem. Mater.*, 2007, **19**, 2395–2397.
- 8 V. L. Budarin, J. H. Clark, R. Luque and D. J. Macquarrie, *Chem. Commun.*, 2007, 634–636.
- 9 J. Ji, G. Zhang, H. Chen, S. Wang, G. Zhang, F. Zhang and X. Fan, *Chem. Sci.*, 2011, **2**, 484–487.
- 10 M. M. Antunes, P. A. Russo, P. V. Wiper, J. M. Veiga, M. Pillinger, L. Mafra, D. V. Evtuguin, N. Pinna and A. A. Valente, *ChemSusChem*, 2014, **7**, 804–812.
- 11 S. Suganuma, K. Nakajima, M. Kitano, S. Hayashi and M. Hara, *ChemSusChem*, 2012, **5**, 1841–1846.
- 12 W.-Y. Lou, Q. Guo, W.-J. Chen, M.-H. Zong, H. Wu and T. J. Smith, *ChemSusChem*, 2012, **5**, 1533–1541.
- 13 X. Qi, H. Guo, L. Li and R. L. Smith Jr, *ChemSusChem*, 2012, **5**, 2215–2220.
- 14 J. Wang, W. Xu, J. Ren, X. Liu, G. Lu and Y. Wang, *Green Chem.*, 2011, **13**, 2678–2681.
- 15 K. Nakajima, M. Okamura, J. N. Kondo, K. Domen, T. Tatsumi, H. Hayashi and M. Hara, *Chem. Mater.*, 2009, **21**, 186–193.



- 16 D. Nandan, P. Sreenivasulu, S. K. Saxena and N. Viswanadham, *Chem. Commun.*, 2011, **47**, 11537–11539.
- 17 J. A. Maciá-Agulló, M. Sevilla, M. A. Diez and A. B. Fuertes, *ChemSusChem*, 2010, **3**, 1352–1354.
- 18 R. Liu, J. Chen, X. Huang, L. Chen, L. Ma and X. Li, *Green Chem.*, 2013, **15**, 2895–2903.
- 19 B. Hu, K. Wang, L. Wu, S.-H. Yu, M. Antonietti and M. M. Titirici, *Adv. Mater.*, 2010, **22**, 813–828.
- 20 W. Zhang, H. Tao, B. Zhang, J. Ren, G. Lu and Y. Wang, *Carbon*, 2011, **49**, 1811–1820.
- 21 X. Liang, M. Zeng and C. Qi, *Carbon*, 2010, **48**, 1844–1848.
- 22 S. Suganuma, K. Nakajima, M. Kitano, D. Yamaguchi, H. Kato, S. Hayashi and M. Hara, *J. Am. Chem. Soc.*, 2008, **130**, 12787–12793.
- 23 S. Van de Vyver, L. Peng, J. Geboers, H. Schepers, F. de Clippel, C. G. Gommers, B. Goderis, P. A. Jacobs and P. F. Sels, *Green Chem.*, 2010, **12**, 1560–1563.
- 24 X. Mo, D. E. Lopez, K. Suwannakam, Y. Liu, E. Loreto, J. G. Goodwin Jr and C. Lu, *J. Catal.*, 2008, **254**, 332–338.
- 25 J. M. Fraile, E. García-Bordejé and L. Roldán, *J. Catal.*, 2012, **289**, 73–79.
- 26 B. Zhang, J. Ren, X. Liu, Y. Guo, Y. Guo, G. Lu and Y. Wang, *Catal. Commun.*, 2010, **11**, 629–632.
- 27 Y. Zhu, S. Murali, M. D. Stoller, K. J. Ganesh, W. Cai, P. J. Ferreira, A. Pirkle, R. M. Wallace, K. A. Cychosz, M. Thommes, D. Su, E. A. Stach and R. S. Ruoff, *Science*, 2011, **332**, 1537–1541.
- 28 M. J. Illán-Gómez, A. García-García, C. Salinas-Martínez de Lecea and A. Linares-Solano, *Energy Fuels*, 1996, **10**, 1108–1114.
- 29 F. L. Conceição, P. J. M. Carrott and M. M. L. R. Carrott, *Carbon*, 2009, **47**, 1874–1877.
- 30 A. J. Romero-Anaya, M. Ouzzine, M. A. Lillo-Ródenas and A. Linares-Solano, *Carbon*, 2014, **68**, 296–307.
- 31 Y. Roman-Leshkov, C. J. Barrett, Z. Y. Liu and J. A. Dumesic, *Nature*, 2007, **447**, 982–985.
- 32 S. N. Naik, V. V. Goud, P. K. Rout and A. K. Dalai, *Renewable Sustainable Energy Rev.*, 2010, **14**, 578–597.
- 33 J. J. Bozell and G. R. Petersen, *Green Chem.*, 2010, **12**, 539–554.
- 34 A.-L. Marshall and P. J. Alaimo, *Chem.-Eur. J.*, 2010, **16**, 4970–4980.
- 35 O. O. James, S. Maity, L. A. Usman, K. O. Ajanaku, O. O. Ajani, T. O. Siyanbola, S. Sahu and R. Chaubey, *Energy Environ. Sci.*, 2010, **3**, 1833–1850.
- 36 D. M. Alonso, J. Q. Bond and J. A. Dumesic, *Green Chem.*, 2010, **12**, 1493–1513.
- 37 R. Luque, A. Pineda, J. C. Colmenares, J. M. Campelo, A. A. Romero, J. Carlos Serrano-Ruiz, L. F. Cabeza and J. Cot-Gores, *J. Nat. Gas Chem.*, 2012, **21**, 246–250.
- 38 J. Zhang, S. Wu, B. Li and H. Zhang, *ChemCatChem*, 2012, **4**, 1230–1237.
- 39 K. S. Arias, S. I. Al-Resayes, M. J. Climent, A. Corma and S. Iborra, *ChemSusChem*, 2013, **6**, 123–131.
- 40 D. J. Hayes, *Catal. Today*, 2009, **145**, 138–151.
- 41 B. C. Windom, T. M. Lovestead, M. Mascal, E. B. Nikitin and T. J. Bruno, *Energy Fuels*, 2011, **25**, 1878–1890.
- 42 R. L. V. Mao, Q. Zhao, G. Dim and D. Petraccone, *Catal. Lett.*, 2011, **141**, 271–276.
- 43 E. Christensen, A. Williams, S. Paul, S. Burton and R. L. McCormick, *Energy Fuels*, 2011, **25**, 5422–5428.
- 44 M. Mascal and E. B. Nikitin, *Angew. Chem., Int. Ed.*, 2008, **47**, 7924–7926.
- 45 X. Hu and C.-Z. Li, *Green Chem.*, 2011, **13**, 1676–1679.
- 46 M. Balakrishnan, E. R. Sacia and A. T. Bell, *Green Chem.*, 2012, **14**, 1626–1634.
- 47 H. Zhu, Q. Cao, C. Li and X. Mu, *Carbohydr. Res.*, 2011, **346**, 2016–2018.
- 48 A. J. Sanborn and S. J. Howard, *US 2009/0156841 A1*, 2009.
- 49 C. M. Lew, N. Rajabbeigi and M. Tsapatsis, *Ind. Eng. Chem. Res.*, 2012, **51**, 5364–5366.
- 50 A. J. Sanborn, *WO 2006/063220 A2*, 2006.
- 51 G. J. M. Gruter and L. E. Manzer, *US 2010/0058650 A1*, 2010.
- 52 H. Wang, T. Deng, Y. Wang, X. Cui, Y. Qi, X. Mu, X. Hou and Y. Zhu, *Green Chem.*, 2013, **15**, 2379–2383.
- 53 X. Hu, R. Gunawan, D. Mourant, C. Lievens, X. Li, S. Zhang, W. Chaiwat and C.-Z. Li, *Fuel*, 2012, **97**, 512–522.
- 54 P. Che, F. Lu, J. Zhang, Y. Huang, X. Nie, J. Gao and J. Xu, *Bioresour. Technol.*, 2012, **119**, 433–436.
- 55 P. Lanzafame, D. M. Temi, S. Perathoner, G. Centi, A. Macario, A. Aloise and G. Giordano, *Catal. Today*, 2011, **175**, 435–441.
- 56 G. M. G. Maldonado, R. S. Assary, J. A. Dumesic and L. A. Curtiss, *Energy Environ. Sci.*, 2012, **5**, 8990–8997.
- 57 J.-P. Lange, W. D. van de Graaf and R. J. Haan, *ChemSusChem*, 2009, **2**, 437–441.
- 58 P. Neves, M. M. Antunes, P. A. Russo, J. P. Abrantes, S. Lima, A. Fernandes, M. Pillinger, S. M. Rocha, M. F. Ribeiro and A. A. Valente, *Green Chem.*, 2013, **15**, 3367–3376.
- 59 P. Neves, S. Lima, M. Pillinger, S. M. Rocha, J. Rocha and A. A. Valente, *Catal. Today*, 2013, **218**, 76–84.
- 60 W. D. V. D. Graaf and J.-P. Lange, *US 2007/7265239 B2*, 2007.
- 61 H. Nishihara, Y. Fukura, K. Inde, K. Tsuji, M. Takeuchi and T. Kyotani, *Carbon*, 2008, **46**, 48–53.
- 62 R. M. Silverstein and F. X. Webster, *Spectrometric Identification of Organic Compounds*, John Wiley & Sons, New York, 6th edn, 1998.
- 63 L. Adams, A. Oki, T. Grady, H. McWhinney and Z. Luo, *Phys. E*, 2009, **41**, 723–728.
- 64 S. Shylesh, S. Sharma, S. P. Mirajkar and A. P. Singh, *J. Mol. Catal. A: Chem.*, 2004, **212**, 219–228.
- 65 J. F. Moulder, W. F. Strickle, P. E. Sobol and K. D. Bomben, *Handbook of X-ray Photoelectron Spectroscopy*, Perkin-Elmer Corporation (Physical Electronics), Eden Prairie, Minnesota, 1992.
- 66 W. H. Lee, J. Y. Kim, Y. K. Ko, P. J. Reucroft and J. W. Zondlo, *Appl. Surf. Sci.*, 1999, **141**, 107–113.
- 67 A. Zheng, S.-J. Huang, S.-B. Liu and F. Deng, *Phys. Chem. Chem. Phys.*, 2011, **13**, 14889–14901.
- 68 Q. Zhao, W.-H. Chen, S.-J. Huang, Y.-C. Hu, H.-K. Lee and S.-B. Liu, *J. Phys. Chem. B*, 2002, **106**, 4462–4469.
- 69 A. Zheng, S.-J. Huang, W.-H. Chen, P.-H. Hu, H. Zhang, H.-K. Lee, L.-C. de Ménorval, F. Deng and S.-B. Liu, *J. Phys. Chem. A*, 2008, **112**, 7349–7356.



- 70 J. Jae, G. A. Tompsett, A. J. Foster, K. D. Hammond, S. M. Auerbach, R. F. Lobo and G. W. Huber, *J. Catal.*, 2011, **279**, 257–268.
- 71 A. Ranoux, K. Djanashvili, I. W. C. E. Arends and U. Hanefeld, *ACS Catal.*, 2013, **3**, 760–763.
- 72 X. Hu, C. Lievens, A. Larcher and C.-Z. Li, *Bioresour. Technol.*, 2011, **102**, 10104–10113.
- 73 G.-J. Gruber and E. de Jong, *Biofuels Technol.*, 2009, **1**, 11–17.
- 74 G. Wang, Z. Zhang and L. Song, *Green Chem.*, 2014, **16**, 1436–1443.

